Hybrid and conventional mesons in the flux tube model: Numerical studies and their phenomenological implications

T. Barnes
Computational and Theoretical Physics Group, Oak Ridge National Laboratory, Oak Ridge, Tennessee 37831-6373 and Department of Physics and Astronomy, University of Tennessee Knoxville, Tennessee 37996-1200

F.E. Close
Daresbury Rutherford Appleton Laboratory, Chilton, Didcot, Oxon OX11 0QX, England

E.S. Swanson
Department of Physics, North Carolina State University, Raleigh, North Carolina 27695-8202
(Received 1 February 1995)

We present results from analytical and numerical studies of a flux tube model of hybrid mesons. Our numerical results use a Hamiltonian Monte Carlo algorithm and so improve on previous analytical treatments, which assumed small flux tube oscillations and an adiabatic separation of quark and flux tube motion. We find that the small oscillation approximation is inappropriate for typical hadrons and that the hybrid mass is underestimated by the adiabatic approximation. For physical parameters in the "one-bead" flux tube model we estimate the lightest hybrid masses (${}_\Lambda L = {}_1P$ states) to be 1.8–1.9 GeV for $u\bar{u}$ hybrids, 2.1–2.2 GeV for $s\bar{s}$, and 4.1–4.2 GeV for $c\bar{c}$. We also determine masses of conventional $q\bar{q}$ mesons with $L = 0$ to $L = 3$ in this model, and confirm good agreement with experimental J-averaged multiplet masses. Mass estimates are also given for hybrids with higher orbital and flux tube excitations. The gap from the lightest hybrid level (${}_1P$) to the first hybrid orbital excitation (${}_1D$) is predicted to be ≈ 0.4 GeV for light quarks ($q = u, d$) and ≈ 0.3 GeV for $q = c$. Both ${}_1P$ and ${}_1D$ hybrid multiplets contain the exotics 1^{-+} and 2^{+-}; in addition the ${}_1P$ has a 0^{+-} and the ${}_1D$ contains a 3^{-+}. Hybrid mesons with doubly excited flux tubes are also considered. The implications of our results for spectroscopy are discussed, with emphasis on charmonium hybrids, which may be accessible at facilities such as BEPC, KEK, a Tau-Charm Factory, and in ψ production at hadron colliders.

PACS number(s): 12.39.Mk, 12.39.Jh

I. INTRODUCTION

The QCD Lagrangian contains quarks and gluons and the successes of perturbative QCD confirm their existence as dynamical degrees of freedom. The behavior of QCD in the strongly interacting low-energy regime, "nonperturbative QCD," is less well understood. Studies using lattice gauge theory have confirmed the presence of confinement and give spectra for conventional mesons and baryons that are in reasonable agreement with experiment [1], but the status of gluonic hadrons in the spectrum has remained obscure.

It is possible that this is now about to change. Candidates for gluonic hadrons have recently been reported which have much in common with theoretical expectations. There are various lattice predictions for the masses of glueballs; the most reliable is presumably for the glueball ground state, which is expected to be a scalar with a mass near 1.5–1.7 GeV [1]. A candidate for the scalar glueball has been reported at 1520 MeV by the Crystal Barrel Collaboration at LEAR [2] and may also be evident in central production by NA12/2 [3] at CERN. Possible evidence for a 1^{-+} light exotic hybrid candidate has been reported in $\rho\pi$ and $f_2\pi$ at about 1775 MeV [4] in $\eta\pi$ and especially $\eta'\pi$ at ~ 1.6 GeV by the VES Collaboration [5], and in $f_1\pi$ [6] with a resonant phase in the region 1.6–2.2 GeV, with production and decay characteristics similar to theoretical expectations for "hybrid" states. A light 1^{-+} signal in $\eta\pi$ reported by the GAMS Collaboration near 1.4 GeV [7] has been withdrawn, although KEK [8] reports a resonant 1^{-+} amplitude with a mass and width similar to the $a_2(1320)$. Another possibility is that the surprisingly large ψ' production at the Fermilab Tevatron [9] may be due to the formation and decay of metastable hybrid charmonium [10].

In view of the discovery of these candidates for gluonic hadrons it is appropriate to investigate the theoretical models for these states more carefully, to see if the predictions are relatively stable and what level of theoretical uncertainty is present. This paper concentrates on hybrid states, which are formed by combining a gluonic excitation with quarks.

Hybrids have been studied in the literature using the flux tube model [11–18], the MIT bag model [19], an adiabatic heavy-quark bag model [20], constituent gluon models [21,22], and heavy-quark lattice gauge theory [23]. In all these approaches the lightest glueball and hybrids (H_q, involving u, d, s flavors) are predicted to have masses in the $\approx 1\frac{1}{2}$–2 GeV region. Hybrids are very attractive experimentally since they span complete flavor nonets

and are expected to include the lightest J^{PC} exotics (which are forbidden to $q\bar{q}$). For recent reviews of hybrids see [24].

Detailed predictions for hybrid spectroscopy were first carried out using the MIT bag model and QCD sum rules. The bag model predictions [19] suffer from parameter uncertainties and possibly additional effects such as gluon self-energies, so the absolute mass scale and the scale of multiplet splittings are somewhat problematical. Conclusions of the bag model studies include the existence of a lightest hybrid meson multiplet at ~ 1.5 GeV and the presence of a 1^{-+} J^{PC} exotic state in this multiplet. In the bag model the lowest $q\bar{q}g$ hybrids have negative parity due to the bag boundary conditions, which give the first TE gluon mode ($J^P = 1^+$) lower energy than TM ($J^P = 1^-$). For heavy quarks it is unrealistic to assume a spherical bag, so Hasenfratz *et al.* [20] introduced an adiabatic bag model in which the bag was allowed to deform in the presence of fixed $Q\bar{Q}$ sources. The resulting $E(R)$ was used in the two-body Schrödinger equation to give mass estimates for hybrids. Masses found for the lightest hybrids were ≈ 3.9 GeV for $c\bar{c}$ (taken from their Fig. 2) and 10.49 GeV for $b\bar{b}$. The estimated systematic uncertainty for $b\bar{b}$ hybrids was ± 0.2 GeV.

QCD sum rules have been applied to the study of hybrids, notably the 1^{-+} and 0^{--} exotics, by several collaborations [25–29]. Early results by these collaborations suggested a light 1^{-+} exotic hybrid with a mass between ≈ 1 GeV and ≈ 1.7 GeV. The 0^{--} exotics were predicted to lie much higher, at 3.1–3.65 GeV. Unfortunately, much of the more recent work is not consistent with these results, although Balitsky, Dyakonov, and Yung [25] continue to support a mass of $M(1^{-+}) \sim 1.5$ GeV. Latorre, Pascual, and Narison [26] cite higher masses of ≈ 2.1 GeV for the u, d 1^{-+} and ≈ 3.8 GeV for the 0^{--}. Govaerts *et al.* [27] estimate ≈ 2.5 GeV for the 1^{-+} $q\bar{q}g$ ($q = u, d, s$), and their other exotic hybrid mass estimates are rather higher than previous references. They conclude however that the sum rules for exotic hybrids are unstable, so all these results are suspect. For heavy 1^{-+} hybrids Narison [26] estimates 4.1 GeV for $c\bar{c}$ and 10.6 GeV for $b\bar{b}$. In contrast, Govaerts *et al.* find ≈ 4.4–5.3 GeV for $c\bar{c}$ and ≈ 10.6–11.2 GeV for $b\bar{b}$, *albeit* with reservations regarding the stability of these results. Thus, sum rules have reached no clear consensus regarding the masses of hybrids, and recent results suggest rather higher masses than previously thought. Some technical errors in the earlier sum rule calculations have been reported by Govaerts *et al.* [28]. Sum rule calculations of decay couplings have also been reported; deViron and Govaerts [29] anticipate a strong $\rho\pi$ decay mode for the $I = 1$, 1^{-+} exotic.

Constituent gluon models for hybrids were introduced by Horn and Mandula [21] and were subsequently developed by Tanimoto, Iddir *et al.*, and Ishida *et al.* [22]. Since these models assume a diagonal gluon angular momentum ℓ_g, their predictions for quantum numbers differ somewhat from the other models. For the lightest hybrid states (with $\ell_g = 0$) Horn and Mandula predict nonexotic quantum numbers equivalent to P-wave $q\bar{q}$ states, since the gluon has $J^P = 1^-$. Exotic quantum numbers including 1^{-+} are predicted in the higher-lying $(\ell_{q\bar{q}}, \ell_g) = (1, 0)$ and $(0, 1)$ multiplets. Detailed spectroscopic predictions for hybrids have not been published using constituent gluon models, and the estimated masses are assigned large uncertainties. A typical result, due to Ishida *et al.*, is 1.3–1.8 GeV for light nonexotic hybrids and 1.8–2.2 GeV for light exotics. This type of model predicts that the dominant two-body decay modes of light exotic hybrids such as 1^{-+} are the $S + P$ combinations [22] such as $b_1\pi$ and $a_1\pi$. This conclusion was subsequently supported by studies of the flux tube model.

Lattice QCD will presumably give the most reliable predictions for absolute hybrid masses, although at present this approach has little to say about multiplet splittings. In heavy-quark lattice QCD, in which the $Q\bar{Q}$ pair is fixed spatially and the gluonic degrees of freedom are allowed to be excited, the lightest charmonium hybrid was predicted by Perantonis and Michael [23] to have a mass of $m(H_c)_{\text{quenched}} = 4.04(3)$ GeV. This reference adds an estimated shift of 0.15 GeV to compensate for the quenched approximation, which leads to a final lattice estimate of $m(H_c) = 4.19$ GeV. Note that a wide range of charm quark masses has been assumed in hybrid spectrum calculations; in this (HQLGT) result a value of $m_c = 1.32$ GeV was used, whereas the flux tube calculations of Isgur, Merlin and Paton [12–14] used $m_c = 1.77$ GeV. The sensitivity of the hybrid mass spectrum to m_c will be addressed subsequently. The corresponding HQLGT estimates for $b\bar{b}$ hybrids were $m(H_b)_{\text{quenched}} = 10.56(3)$ GeV and $m(H_b) = 10.81$ GeV.

In the flux tube model the more recent calculations [12–14] cite masses of about 1.9 GeV for the lightest ($q = u, d$) hybrid multiplet, about 4.3 GeV for $c\bar{c}$ hybrids, and about 10.8 GeV for $b\bar{b}$ hybrids. There is an overall variation of about 0.2–0.3 GeV in these predictions, as indicated in Table I. Although multiplet splittings are usually neglected in the flux tube model, a rather large inverted spin-orbit Thomas term was found by Merlin and Paton [14]. The flux tube model also predicts very characteristic two-body decay modes for hybrids [16,17] which have motivated experimental studies of the channels $f_1\pi$ and $b_1\pi$, and suggest $h_1\pi$ and $\rho\pi$ [17] as interesting future possibilities.

The mass predictions for the lowest-lying (1^{-+}) exotic hybrid (which is essentially the mass of the lightest hybrid multiplet) are summarized in Table I.

In this paper we carry out improved numerical studies of the flux tube model, which is the most widely cited model for hybrids. Previous flux tube estimates of the hybrid spectrum made several simplifying assumptions, including a small oscillation approximation and an adiabatic separation of quark and flux tube motion [11–15]. In principle these could introduce important systematic biases in the spectrum. We will present numerical results which are free of these approximations, using a Hamiltonian Monte Carlo technique. Since our results for the lightest hybrid masses are quite similar to previous analytical results, we conclude that the approximations made were reasonable, or when they did lead to important numerical inaccuracies (such as in the adia-

TABLE I. Predicted 1^{-+} hybrid masses.

State	mass (GeV)	Model	Ref.
$H_{u,d}$	1.3–1.8	Bag model	[19]
	1.8–2.0	Flux tube model	[11–14]
	2.1–2.5	QCD sum rules (most after 1984)	[26–28]
H_c	≈ 3.9	Adiabatic bag model	[20]
	4.2–4.5	Flux tube model	[12–14]
	4.1–5.3	QCD sum rules (most after 1984)	[26–28]
	4.19(3) $\pm$ syst.	HQLGT	[23]
H_b	10.49(20)	Adiabatic bag model	[20]
	10.8–11.1	Flux tube model	[12–14]
	10.6–11.2	QCD sum rules (most after 1984)	[26–28]
	10.81(3) $\pm$ syst.	HQLGT	[23]

batic approximation and in the small oscillation approximation at small R) the estimates of corrections to the approximations were sufficiently accurate. Thus, we substantiate previous estimates of hybrid masses in the flux tube model, and we also give masses for higher hybrid excitations using our techniques.

II. THE FLUX TUBE MODEL

A. Definitions

In lattice QCD widely separated static color sources are confined by approximately cylindrical regions of chaotic color fields [31]. The flux tube model is an attempt to describe this phenomenon with a simple dynamical model, and was motivated by the strong-coupling expansion of lattice QCD [11] and by early descriptions of flux tubes as cylindrical bags of colored fields [32]. In this model one approximates the confining region between quarks by a string of mass points, "beads," with a confining potential between the beads. Since a line of flux in strong-coupling LGT can be extended only in transverse directions (by the application of plaquette operators), by analogy in the flux tube model one allows only locally transverse spatial fluctuations of the bead positions. For a string of N mass points which connects a quark at site 0 to an antiquark at site $N+1$ we write the flux tube model Hamiltonian as

$$H = H_{\text{quarks}} + H_{\text{flux tube}} , \tag{1}$$

$$H_{\text{quarks}} = -\frac{1}{2m_q}\vec{\nabla}_q^2 - \frac{1}{2m_{\bar{q}}}\vec{\nabla}_{\bar{q}}^2 + V_{q\bar{q}} , \tag{2}$$

$$H_{\text{flux tube}} = -\frac{1}{2m_b}\sum_{i=1}^{N}\left(\sum_{\hat{\eta}_T}(\hat{\eta}_T\cdot\vec{\nabla}_i)^2\right) + \sum_{i=1}^{N+1} V\left(|\vec{r}_i - \vec{r}_{i-1}|\right) . \tag{3}$$

Here m_q and $m_{\bar{q}}$ are the quark and antiquark masses, m_b is the bead mass, and the $\{\hat{\eta}_T\}$ are two orthogonal unit vectors associated with bead i that are transverse to the local string tangent $(\vec{r}_{i+1}-\vec{r}_{i-1})/|\vec{r}_{i+1}-\vec{r}_{i-1}|$. In this study we use a standard linear form for the string potential,

$$V\left(|\vec{r}_i - \vec{r}_{i-1}|\right) = a|\vec{r}_i - \vec{r}_{i-1}| , \tag{4}$$

and we usually set the string tension a equal to 1.0 GeV/fm. For our estimates of physical hybrid masses we will augment this with a color Coulomb interaction for $V_{q\bar{q}}$ in (2).

B. Adiabatic potentials and flux tube parameters

In the flux tube studies of Isgur, Kokoski, Merlin, and Paton [11–16] the combined quark and flux tube system is treated using an adiabatic approach as a zeroth order approximation. In the adiabatic analysis one exploits the anticipated fast dynamical response of the flux tube relative to heavy-quark time scales, and separates the flux tube and quark degrees of freedom. This is accomplished by fixing the $q\bar{q}$ separation at R and determining an eigenenergy $E_\Lambda(R)$ of the flux tube. Solution of the Schrödinger equation for the $q\bar{q}$ wavefunction in the flux tube ground state potential $E_0(R)$ then gives the conventional $q\bar{q}$ meson spectrum in the adiabatic approximation. Hybrids are excited states of the string in this approach, and are found using an excited string potential $E_\Lambda(R)$. The lightest hybrid follows from an $E_1(R)$ in which the lowest string mode has a single orbital excitation about the $q\bar{q}$ axis.

In previous studies the adiabatic potentials $\{E_\Lambda(R)\}$ were determined *assuming small string fluctuations relative to the $q\bar{q}$ axis.* We shall find that this is an inaccurate approximation for typical hadrons, assuming $R \approx 1$ fm.

One motivation for the small oscillation approximation is that it leads to relatively simple analytical results; when applied to (3) it gives a quadratic Hamiltonian, which can be diagonalized using Fourier modes. To illustrate this, consider a string with fixed ends at $\mathbf{x}_0 = (0,0,0)$ and $\mathbf{x}_{N+1} = (0,0,R)$ and N dynamical beads, with motion allowed only in the transverse $\{x_i, y_i\}$

directions. In the small oscillation approximation, assuming that the beads are equally spaced in z by a_0, so $z_n = na_0$ and $a_0 = R/(N+1)$, the flux tube Hamiltonian becomes

$$H_{\text{flux tube}} = aR - \frac{1}{2m_b}\sum_{i=1}^{N}\left(\frac{\partial^2}{\partial x_i^2}+\frac{\partial^2}{\partial y_i^2}\right) + \frac{a/a_0}{2}\sum_{i=1}^{N+1}[(x_i-x_{i-1})^2+(y_i-y_{i-1})^2] \ . \tag{5}$$

This is equivalent to a system of N coupled masses $\{m_b\}$ with an effective spring constant of $k = a/a_0 = (N+1)a/R$. We can diagonalize this using sine variables

$$s_{n,\lambda=(1,2)} = \sqrt{\frac{2}{N+1}}\sum_{i=1}^{N}\sin(k_n z_i)\,(x,y)_i \tag{6}$$

and

$$(x,y)_i = \sqrt{\frac{2}{N+1}}\sum_{n=1}^{N}\sin(k_n z_i)\,s_{n,\lambda=(1,2)} \tag{7}$$

where $k_n = \pi n/R$. This gives

$$H_{\text{flux tube}} = aR + \sum_{n=1}^{N}\sum_{\lambda=1}^{2}\left(-\frac{1}{2m_b}\frac{\partial^2}{\partial s_{n\lambda}^2}+\frac{1}{2}\kappa_n s_{n\lambda}^2\right), \tag{8}$$

where the effective spring constant of the nth Fourier mode is

$$\kappa_n = \frac{4(N+1)a}{R}\sin^2\left(\frac{\pi n}{2(N+1)}\right) . \tag{9}$$

The ground state energy of the string, which is used as the adiabatic potential for conventional $(q\bar{q})$ mesons, is aR plus the sum of $\omega/2$ for each mode in the small oscillation approximation. The individual eigenfrequencies are

$$\omega_n = \sqrt{\kappa_n/m_b} = 2\sqrt{\frac{(N+1)a}{m_b R}}\sin\left(\frac{\pi n}{2(N+1)}\right) , \tag{10}$$

and the mode sum runs over $n = 1$ to N and $\lambda = 1, 2$. The resulting ground state energy is

$$E_0(R) = aR + \sum_{\text{modes}}\frac{1}{2}\omega_n = aR + \sqrt{\frac{2(N+1)a}{m_b R}}\left\{\frac{\sin\left(\frac{\pi N}{4(N+1)}\right)}{\sin\left(\frac{\pi}{4(N+1)}\right)}\right\} , \tag{11}$$

which agrees with the result of Isgur and Paton [11]. The most general adiabatic potential in the small oscillation approximation is

$$E(R) = E_0(R) + \sum_{\substack{\text{modes}\\ n}} n_n\,\omega_n(R) \ , \tag{12}$$

where n_n is the number of excitations of the mth flux tube mode.

The ground state wave function of the string in the small oscillation approximation is a Gaussian in the Fourier mode amplitudes,

$$\Psi_0(\{x_i,y_i\}) = \prod_{n,\lambda}\eta_n\, e^{-s_{n\lambda}^2/2\sigma_n^2} \ , \tag{13}$$

where the Gaussian width of mode n,λ is given by

$$\sigma_n = \frac{1}{\sqrt{m_b\omega_n}} = \frac{\left[\frac{R}{(N+1)am_b}\right]^{1/4}}{\left[2\sin\left(\frac{\pi n}{2(N+1)}\right)\right]^{1/2}} . \tag{14}$$

This suggests an estimate of the range of validity of the small oscillation approximation; it should fail when these fluctuations become comparable to R.

Excitations can be created from the ground state wavefunction (13) through the application of "phonon" creation operators

$$A_{n,\lambda}^{\dagger} = \frac{1}{\sqrt{2m_b\omega_n}}\left(-\frac{\partial}{\partial s_{n\lambda}}+m_b\omega_n s_{n\lambda}\right) , \tag{15}$$

with an increase in energy of ω_n. States with definite angular momentum component Λ along the $q\bar{q}$ axis, which are useful in constructing hybrid states, are created by the linear combinations

$$A_{n,\Lambda=\pm1}^{\dagger} = \frac{1}{\sqrt{2}}\left(\mp A_{n,1}^{\dagger} - iA_{n,2}^{\dagger}\right) . \tag{16}$$

The flux tube parameters a, m_b, and N can be constrained by the plausible requirement that the maximum propagation velocity on the flux tube be c. In the large-N limit this implies [from (10)]

$$v_{\max}/c \equiv \lim_{k\to 0}\frac{\partial\omega}{\partial k} = \sqrt{\frac{aa_0}{m_b}} = 1 \ . \tag{17}$$

The length a_0 might reasonably be identified with the transverse flux tube extent of $\approx$ 0.2–0.3 fm found in a lattice Hamiltonian string theory [30] or the $\approx$ 0.2–0.4 fm estimated in lattice Monte Carlo QCD [31]. For a typical string tension of $a = 1.0$ GeV/fm the constraint (17) implies $m_b \approx 0.2$–0.4 GeV. We take $m_b = 0.2$ GeV as our standard value, since the larger transverse extent of 0.4 fm may represent fluctuations of an intrinsically smaller flux tube.

Isgur, Merlin, and Paton [11–16] also treat a_0 as a fundamental length but allow N to vary continuously with

R, so that $a_0 = R/(N+1)$ is constant. The large-R hybrid potential gap of

$$\lim_{R\to\infty} \omega_1(R) = \sqrt{\frac{a}{m_b}}\,\frac{\pi}{\sqrt{(N+1)R}} \tag{18}$$

then becomes

$$\lim_{R\to\infty} \omega_1(R) = \sqrt{\frac{aa_0}{m_b}}\,\frac{\pi}{R} = \frac{\pi}{R}\,. \tag{19}$$

The final result follows from the constraint (17). An excitation energy of π/R was found earlier by Gnädig *et al.* [32] in their cylindrical bag model of a flux tube.

Of course we cannot vary N continuously in a numerical simulation. In this first numerical study we shall mainly consider the simplest fixed-N case, $N = 1$. As we shall see, this allows a detailed study of the various approximations used previously in estimating hybrid masses, and leads to very plausible results for conventional and hybrid spectroscopy. For the sake of completeness we also discuss some $N > 1$ Monte Carlo results in a footnote to Sec. V.

III. NUMERICAL RESULTS FOR ADIABATIC POTENTIALS

We will now generate adiabatic potentials numerically, for comparison with the small oscillation potentials derived in the previous section.

The adiabatic $N = 1$ (single bead) problem can be integrated numerically, since there is only motion in a single plane, and the bead wavefunction can be separated as $\Psi_\Lambda(\rho,\theta) = \psi_\Lambda(\rho)\exp(i\Lambda\theta)$. The ordinary differential equation satisfied by $\psi_\Lambda(\rho)$ is

$$-\frac{1}{2m_b}\left(\frac{d^2\psi_\Lambda}{d\rho^2} + \frac{1}{\rho}\frac{d\psi_\Lambda}{d\rho}\right)$$

$$+\left(2a\sqrt{\rho^2+R^2/4} + \frac{\Lambda^2}{2m_b\rho^2}\right)\psi_\Lambda = E_\Lambda(R)\psi_\Lambda\,, \tag{20}$$

and the exact $q\bar{q}$ meson adiabatic potential $E_0(R)$ and first hybrid adiabatic potential $E_1(R)$ follow from solving this equation for its lowest eigenvalue with $\Lambda = 0$ and $\Lambda = 1$, respectively. The potentials $E_0(R)$ and $E_1(R)$ and the potential gap $E_1(R) - E_0(R)$ are shown in Figs. 1 and 2 for $m_b = 0.2$ GeV and $a = 1.0$ GeV/fm. In the limit of infinitely massive quarks the adiabatic approximation is exact, the $Q\bar{Q}$ separation approaches zero, and the hybrid mass gap is therefore $E_1(0) - E_0(0)$ ($= 0.829$ GeV with these parameters). As R increases the potential gap falls, but asymptotically as $2\sqrt{a/m_bR}$ [(10) with $n = 1$ and $N = 1$] rather than as the π/R of Isgur and Paton, due to our assumption of a fixed-N flux tube. The small oscillation adiabatic potentials and gap from (10)–(12) are shown as dashed lines in Figs. 1 and 2; they are evidently useful only beyond $R \approx 1$ fm. Since $R \approx 1$ fm is a typical light (u,d,s) hadron length scale, the small oscillation approximation is inappropriate for light hadrons. For smaller R the approximate small oscillation adiabatic potentials depart considerably from the true $\{E_\Lambda(R)\}$ (solid lines), and actually diverge as $R \to 0$.

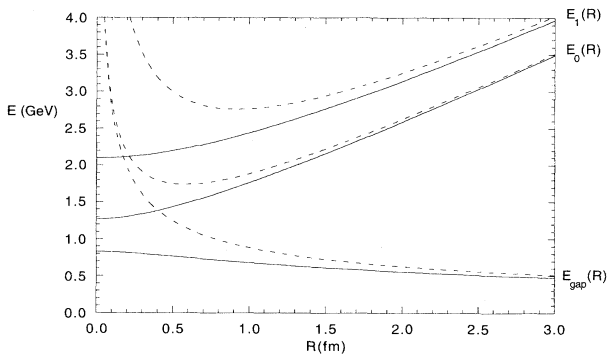

FIG. 1. Ground state and first hybrid adiabatic potentials and their difference, for $N = 1$. Solid lines are exact and dashed lines are the small oscillation approximation. String tension $a = 1.0$ GeV/fm, bead mass $m_b = 0.2$ GeV.

In the previous section we suggested a condition for applicability of the small oscillation approximation, which is that R should be much larger than the zero-point fluctuations σ_n in the string ground state. The largest fluctuations are in the $n = 1$ mode; taking this case, the mode width for $N = 1$ is

$$\sigma_1 = \left[\frac{R}{4m_ba}\right]^{1/4}. \tag{21}$$

Note the weak parameter dependence of the scale of fluctuations implied by the 1/4 power. The characteristic length R_c at which the scale of fluctuations σ_1 equals R is given by

$$R_c(N=1) = (4m_ba)^{-1/3} = 0.37 \text{ fm}. \tag{22}$$

R should be significantly larger than this for the small oscillation approximation to be useful, which is supported by our Figs. 1 and 2.

Although this paper is primarily concerned with nu-

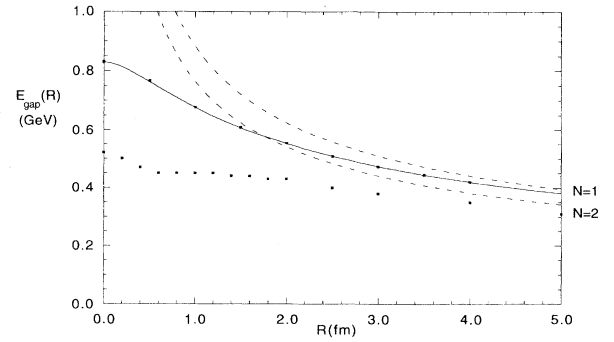

FIG. 2. Hybrid potential gap $E_1(R) - E_0(R)$ for $N = 1$ and $N = 2$. Plotting conventions and parameters as in Fig. 1; points are Monte Carlo data.

merical results for the $N = 1$ one-bead flux tube model, we can carry out simulations for larger N using a Hamiltonian Monte Carlo technique [33]. This method will be discussed in the next section, in which it is applied to the combined dynamical quark and flux tube system. As a test of the Monte Carlo method we confirmed that the adiabatic potentials $E_0(R)$ and $E_1(R)$ with $N = 1$ are accurately reproduced (Fig. 2), and we also show results for the $N = 2$ case. The hybrid mass gap falls with increasing N, so it may be difficult to find a realistic description of the spectrum with a fixed-N flux tube model for large N; the excitation energy of a many-bead string is presumably quite low relative to the $N = 1$ case, assuming similar m_b and a. There are also rather subtle complications in the dynamics of the $N > 1$ flux tube with fixed ends; the constraint of transverse bead motion implies dependence of energies on the initial conditions, which must then be varied to find the lowest-lying state.

IV. HYBRIDS WITH DYNAMICAL QUARKS

A. Adiabatic results

Thus far we have only considered the adiabatic potentials. Now we shall solve the two-body $q\bar{q}$ Schrödinger equation in the exact adiabatic potentials $\{E_\Lambda(R)\}$, which are determined by numerically integrating (20) for a flux tube with static sources separated by R. The flux tube ground state and first excited state potentials $E_0(R)$ and $E_1(R)$ lead to conventional and the lightest hybrid mesons, respectively.

For hybrids there is a centrifugal barrier for the $q\bar{q}$ pair that arises from the matrix element of $\vec{L}_q^2$ in the full quark and flux tube angular momentum eigenstate. The angular wave function of the combined gluon or flux tube and quark system was discussed by Horn and Mandula [21] and subsequently by Hasenfratz *et al.* [20] and Isgur and Paton [11]. There are discrepancies between these references in the C and P hybrid quantum numbers; this does not affect our conclusions regarding hybrid energies because of degeneracies between the levels concerned. The latter two references give essentially the same rigid body angular wavefunction for the full system, which is

$$\psi_H^{(L)} \propto \mathcal{D}_{M\Lambda}^{(L)}(\phi, \theta, -\phi) \ . \tag{23}$$

(The wavefunction of Hasenfratz *et al.* does not have the final $-\phi$ argument because it uses body-fixed rather than space-fixed coordinates.) This is the amplitude to find the $q\bar{q}$ axis pointing along (θ, ϕ) in a hybrid state with total orbital angular momentum L and $\hat{z}$ projection M, and Λ is the projection of the flux tube orbital angular momentum along the $q\bar{q}$ axis. $\Lambda = \sum_m (n_{m+} - n_{m-})$, where $n_{m\pm}$ is the number of excitations of the mth flux tube mode, $(+)$ for right handed and $(-)$ for left handed, as in (16). Thus for a single flux tube excitation $\Lambda = \pm 1$, for doubly excited flux tubes $\Lambda = 0, \pm 2$, and so forth. Parity implies a degeneracy between $\Lambda = \pm|\Lambda|$ levels, and so without loss of generality we assume nonnegative Λ in our simulations. The total orbital angular momentum L is constrained to be $L \geq |\Lambda|$.

The wave function (23) is not fully diagonal in configuration space; it assumes that the flux tube is in a coherent superposition of orientations about the $q\bar{q}$ axis such that the angular momentum projection Λ along the $q\bar{q}$ axis is diagonal. This requires a wave function

$$\psi_{\text{flux tube}}^{(\Lambda)}(\phi_b) = \frac{1}{\sqrt{2\pi}} e^{i\Lambda\phi_b} \ , \tag{24}$$

where ϕ_b gives the rotation of the flux tube about the $q\bar{q}$ axis relative to a reference configuration. In our Monte Carlo simulation we used basis states which are fully diagonal in coordinate space, so a configuration is defined (for $N = 1$) by the coordinates $\vec{x}_q, \vec{x}_{\bar{q}}, \vec{x}_b$, which implicitly determine its orientation relative to a reference configuration and space-fixed axes, specified by the $q\bar{q}$ axis angles θ, ϕ and the rigid-body rotation angle ϕ_b. This relation is defined by the effect of the rotation operator:

$$|\theta, \phi, \phi_b\rangle = e^{-i\phi J_z} \, e^{-i\theta J_y} \, e^{+i\phi J_z} \, |\hat{z}, \phi_b\rangle \ . \tag{25}$$

The angles θ and ϕ are specified trivially by the $q\bar{q}$ axis. The rigid-body rotation angle ϕ_b is rather more complicated, and satisfies

$$\sin(\phi_b) = \frac{\sin(\phi)(x_b - x_{q\bar{q}\ \text{cog}}) + \cos(\phi)(y_b - y_{q\bar{q}\ \text{cog}})}{|\vec{r}_b - \vec{r}_{q\bar{q}\ \text{cog}}|} \ , \tag{26}$$

as may be confirmed from Fig. 3, which shows the operations required to reach a general configuration from an unrotated "reference" configuration.

Given the ϕ_b dependence implicit in the Λ states, our ϕ_b-diagonal angular wave functions must be of the form

$$\langle \theta, \phi, \phi_b | L, M\Lambda \rangle \propto \mathcal{D}_{M\Lambda}^{(L)}(\phi, \theta, \phi_b - \phi) \ , \tag{27}$$

which we shall use as the guiding wave function for hybrid states in the Monte Carlo simulation.

In their Eq. (28) Isgur and Paton [11] [see also Eq. (6) of Merlin and Paton [12]] introduce a simple approximation for the matrix element of $\vec{L}_q^2$, which neglects a mixing operator that raises and lowers Λ. This approximation gives $\langle \vec{L}_q^2 \rangle \approx L(L+1) - \Lambda^2$, which transforms the Schrödinger equation into an ordinary differential equation for the adiabatic $q\bar{q}$ radial wave function $\psi_\Lambda^{(L)}(r)$:

$$H_{\text{adia}} = -\frac{1}{2\mu}\left(\frac{\partial^2}{\partial r^2} + \frac{2}{r}\frac{\partial}{\partial r}\right) + \frac{L(L+1) - \Lambda^2}{2\mu r^2} + E_\Lambda(r) \ , \tag{28}$$

$$H_{\text{adia}} \psi_\Lambda^{(L)}(r) = M_H \psi_\Lambda^{(L)}(r) \ . \tag{29}$$

Isgur and Paton determined the hybrid spectrum by solving this eigenvalue problem, with an additional approximation; they replaced the singular small oscillation adiabatic potentials $E_\Lambda(R)$ (12) with approximate forms that

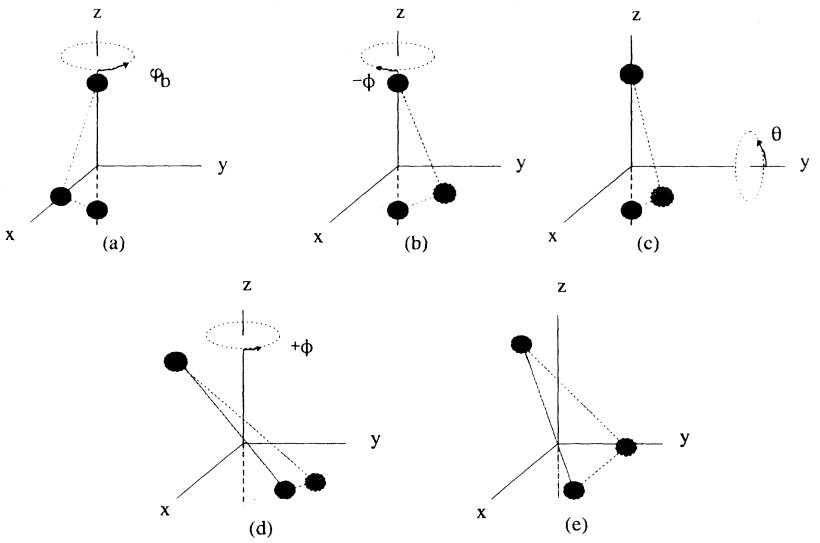

FIG. 3. An $N = 1$ quark, antiquark, and flux tube bead, showing the $q\bar{q}$ axis angles θ and ϕ and the rigid-body rotation angle ϕ_b relative to the reference configuration.

were nonsingular at $R = 0$. We shall instead use the exact (numerical) adiabatic potentials $\{E_\Lambda(R)\}$ [from (20)] in (28),(29) above, which give the true adiabatic result for the spectrum. This will be compared to our Monte Carlo results.

B. Monte Carlo simulation

We improve on previous studies of the flux tube model by using the guided random walk (GRW) Hamiltonian Monte Carlo algorithm [33] to solve the full $N = 1$ model without adiabatic or small oscillation approximations. The GRW algorithm maps the imaginary time Schrödinger equation onto a diffusion problem, which is then solved numerically using weighted random walks in the configuration space of the system. The statistical error is reduced through the use of a guiding wave function for importance sampling, which is used to determine stepping probabilities between configurations during the walk. This importance sampling does not bias the energies and matrix elements.

In this algorithm a random walk is generated by stepping in the coordinates which define configuration space. For a $q, \bar{q}$ and N-bead system there are $N_x = 2N + 6$ possible coordinates to increment. Starting from a specified initial configuration of quark, antiquark, and bead locations at $\tau = 0$, one of the coordinates is chosen at random, and an increment $x \to x + h_q$ (or h_b) is made in that coordinate with probability

$$P(\text{step}) = \frac{1}{2}\frac{\psi_g(x_{\text{new}})}{\psi_g(x_{\text{current}})} . \tag{30}$$

If the move is not accepted, a move in the opposite direction is made, $x \to x - h_q$ (or h_b). The step sizes in h_b (for bead moves) and h_q (for quark or antiquark moves, with m_q and $m_{\bar{q}}$ assumed equal) are given by

$$h_b = \sqrt{\frac{N_x h_\tau}{m_b}} \tag{31}$$

and

$$h_q = \sqrt{\frac{m_b}{m_q}}\, h_b , \tag{32}$$

where h_τ is a small step size in Euclidean time (relative to inverse energy scales). After each move the Euclidean time is incremented by h_τ. Excited states with nodes in the guiding wave function ψ_g require special consideration; for these cases we test that moves do not cross the nodal surface, and if they do they are rejected and another move is generated. This introduces a bias which vanishes as $h_\tau \to 0$. There is also a bias in excited state energies if a guiding wave function which has incorrect nodes is used.

For the static quark simulations in Sec. III we used a guiding wave function which is a Gaussian in the total string length R_{str},

$$\psi_g = \exp\left\{ -(R_{\text{str}}/\xi)^2 \right\} , \tag{33}$$

and allowed only bead moves. The optimum guidance parameter ξ was estimated numerically by minimization of the statistical error, specifically by minimizing the variance of the weight factor $w(\tau)$ in (35). For $N = 1$ and all the R values considered here the optimum value was found to be $\xi \approx 1.5$ fm.

For the dynamical quark ground state we use, as our guiding wave function,

$$\psi_g^{(0)} = \exp\left\{ -(R_{\text{str}}/\xi)^2 - R/\xi_{q\bar{q}} \right\} . \tag{34}$$

This simple generalization of the static quark Gaussian (33) includes a suppression of the wave function with in-

creasing interquark separation R for fixed string length $R_{\rm str}$, as is intuitively expected for heavy quarks. For excited-L $q\bar{q}$ and hybrid states the wave function is more complicated, and must incorporate nodes to ensure orthogonality to the ground state (see below).

In the course of a random walk from Euclidean time 0 to τ we generate a path-dependent weight factor, given by

$$w(\tau) = \exp\left\{ \int_0^\tau \left(-V + \left[\frac{\nabla_q^2 \psi_g + \nabla_{\bar{q}}^2 \psi_g}{2m_q} + \frac{\nabla_b^2 \psi_g}{2m_b} \right] \psi_g^{-1} \right) d\tau \right\} , \tag{35}$$

where the Laplacians are in the 6 quark and antiquark and $2N$ (transverse) bead coordinates, respectively. The form (35) and the step sizes h_b and h_q above are chosen so that a histogram of these weights in configuration space $\{x\}$ is proportional to a solution $\psi(\{x\},\tau)$ of the Euclidean time Schrödinger equation. Actually $w(\tau)$ gives the related function $\psi_g(\{x\})\psi(\{x\},\tau)$ [34]; this $\psi_g\psi$ can also be used to determine the ground state energy, and is generated with a smaller statistical error than ψ itself. The energy is determined from the large-τ behavior of the weight $w(\tau)$: At large τ the walk-averaged weight $\langle w(\tau)\rangle$ approaches an exponential in τ,

$$\lim_{\tau\to\infty} \langle w(\tau)\rangle = \kappa\, e^{-E_0\tau}[1 + O(e^{-E_{gap}\tau})] , \tag{36}$$

so we may determine E_0 from measurements of $\langle w\rangle$ at two successive Euclidean times:

$$E_0 = \lim_{\tau_1,\tau_2\to\infty} \frac{1}{(\tau_2 - \tau_1)} \ln\left\{ \frac{\langle w(\tau_1)\rangle}{\langle w(\tau_2)\rangle} \right\} . \tag{37}$$

In practice we leave $\tau_2 - \tau_1$ fixed and increase τ_1 until the E_0 estimate has converged to the required accuracy.

If a guiding wave function ψ_g with nodes is used, we recover the lowest energy eigenvalue for which $\psi = 0$ on those nodes. If the nodes are identical to those of an excited state ψ_n of the system, we recover the correct E_n from (37).

This algorithm gives the true eigenenergy for any guiding wave function ψ_g with correct nodes, provided that the initial configuration has nonzero amplitude in the ground state. The results become statistically more accurate as the guiding wave function is made closer to the true eigenfunction ψ_n, and one may confirm that the best possible choice is an energy eigenfunction, $\psi_g = \psi_n$ [34]. In this case the weight factor (35) becomes $w = \exp(-E_n\tau)$ exactly for each walk, so the energy can be determined from a single walk at arbitrary τ. Of course we do not know ψ_n in general, so we use a parametrized ansatz for ψ_n as our ψ_g, and determine the optimum parameters numerically by minimizing the variance of the weight factors $\{w\}$ in a sample of random walks. Given the optimized guiding wave function ψ_g, we then determine E_n using (37).

C. Monte Carlo results

For $\alpha_s = 0$ we generated Monte Carlo energies for quark masses of $m_q = 0.33$, 0.5, 1.0, 1.5, 2.5, 5.0, and 10.0 GeV, with a string tension of $a = 1.0$ GeV/fm. The optimized guiding wave function parameters in (34) were $\xi = 1.5$ fm and $\xi_{q\bar{q}} = 1.4$, 1.0, 0.7, 0.6, 0.5, 0.4, and 0.3 fm for the quark masses given above. The Euclidean times used, which were chosen to insure convergence to ground state results to within our statistical errors, were $\tau_1 = 10.0\ \text{GeV}^{-1}$ and $\tau_2 = \tau_1 + 1.0\ \text{GeV}^{-1}$, and the step size was $h_\tau = 0.005\ \text{GeV}^{-1}$. For energy differences of excited and ground state levels, $E_n - E_0$, we found adequate convergence with a smaller time of $\tau_1 = 5.0\ \text{GeV}^{-1}$. We also generated energies for various other guidance and time parameters to confirm the accuracy of these results. The sample size was usually $N_{\rm rw} = 8 \times 1024$ walks (8 separate runs to generate errors), and we used bootstrap on each of the 8 runs to suppress dependence on the initial configuration. (In a bootstrapped run the final configuration of a walk at $\tau = \tau_2$ is used as the initial configuration of the next walk at $\tau = 0$.) For hybrids with $m_q = 0.33$ and 0.5 GeV we used longer runs of $N_{\rm rw} = 8 \times 4096$ walks to compensate for the larger statistical errors.

The adiabatic ground state energies [from (28),(29) with the potential $E_0(R)$ of (20)] and Monte Carlo results for $N = 1$ are summarized in Table II for $\alpha_s = 0$, $m_b = 0.2$ GeV, and $a = 1.0$ GeV/fm.

Evidently the adiabatic approximation considerably underestimates the ground state energy, by up to 0.3 GeV for light (u,d) quark systems. The discrepancy falls rather slowly with increasing quark mass, approximately as $m_q^{-1/4}$.

For excited-L quarkonia we generalize the ground state guiding wave function to

$$\psi_g^{(L)} = \psi_g^{(0)} R^L f(\theta,\phi) , \tag{38}$$

where the angular function depends on the direction of the $q\bar{q}$ axis, and was taken to be the real part of $Y_{LM}(\theta,\phi)$. (The algorithm requires a real wave function for importance sampling.) The radial factor R^L is not essential but is expected to be closer to the true $\psi_0^{(L)}$, and its inclusion reduces our statistical errors somewhat.

TABLE II. Adiabatic and exact (Monte Carlo) ground state energies for $N = 1$.

m_q (GeV)	$E_0^{\rm adia}$ (GeV)	$E_0^{\rm MC} - E_0^{\rm adia}$ (GeV)
0.33	1.985	0.274(4)
0.50	1.868	0.231(5)
1.00	1.711	0.187(3)
1.50	1.638	0.164(3)
2.50	1.563	0.148(3)
5.00	1.484	0.124(2)
10.0	1.425	0.114(3)

For hybrid states the amplitude to find the system at (θ, ϕ, ϕ_b) is given by (27):

$$\psi_H^{(L)}(\theta,\phi,\phi_b) \propto \mathcal{D}^{(L)}_{M\Lambda}(\phi,\theta,\phi_b-\phi) = e^{i\Lambda\phi_b}\, e^{i(M-\Lambda)\phi}\, d^{(L)}_{M\Lambda}(\theta)\ . \tag{39}$$

For our full hybrid guiding wave function we multiply the real part of this angular function by a radial wave function similar to our ground state ψ_g:

$$\psi_g^{(H)} = \psi_g^{(0)} \rho_b\, R f(\theta,\phi,\phi_b)\ , \tag{40}$$

$$f(\theta,\phi,\phi_b) = d^{(L)}_{M\Lambda}(\theta)\, \cos[\Lambda\phi_b + (M-\Lambda)\phi]\ . \tag{41}$$

The product of ρ_b (the bead-axis distance) and R was introduced as a simple centrifugal suppression factor.

There is a systematic bias in our results for excited states due to the nodal surfaces specified by the angular wave functions f; these surfaces are exact only in the limit $m_q \to \infty$. For our high statistics quarkonium simulations we used $M = 0$ states for simplicity. We checked for evidence of node bias by comparing the energies found using guiding wave functions with different magnetic quantum number M, which have different nodal surfaces. The bias in $q\bar{q}$ states was at most about 10 MeV, comparable to our statistical errors. For the $_1P$ hybrid, however, we found a significant M-dependent bias; in Fig. 4 we show hybrid energies determined using both $M = 0$ and $M = 1$ in (41). The largest bias was at the smallest quark mass of $m_q = 0.33$ GeV, for which we found $E(_1P, M = 1) - E(_1P, M = 0) = 52(18)$ MeV. This bias will be discussed in more detail in our treatment of hybrids with physical parameters.

Figure 4 shows the P-wave and D-wave $q\bar{q}$ levels and the first hybrid level ($_\Lambda L = {}_1P$) relative to the ground state energy E_0, using the adiabatic approximation (lines) and the Monte Carlo simulation (points). Our results show that the adiabatic approximation is more accurate for the energy differences $\{E_n - E_0\}$, which are the experimentally observable quantities, than for E_0 itself. The largest discrepancies between adiabatic and Monte Carlo results are ≈ 100 MeV, for the D-wave and hybrid states at the lightest quark mass of 0.33 GeV. Note that the adiabatic approximation *overestimates* the excited-L energies but *underestimates* the hybrid energy. Thus, *if we use the adiabatic approximation and fit the experimental D-wave levels, we underestimate the light hybrid mass by $\approx$ 200 MeV.*

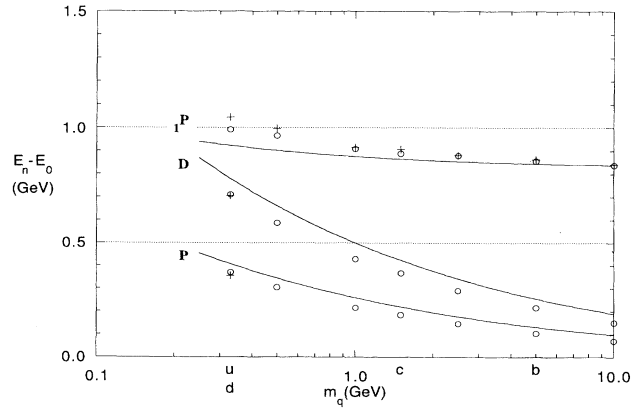

FIG. 4. Energies of the lightest $L = 1, 2$ $q\bar{q}$, and $_\Lambda L = {}_1P$ hybrid states relative to $E_0 = E_S$ for $N = 1$. Lines show the adiabatic approximation and the points are Monte Carlo data, $M = 0$ (open) and $M = L$ (plus). Parameters $m_b = 0.2$ GeV, $a = 1.0$ GeV/fm, $\alpha_s = 0$.

In their analytical study of the flux tube model, Merlin and Paton [12] also found that postadiabatic corrections reduce the excited-L energies and increase the hybrid energy. They find ($q = u, d$) P, D and $_1P$ hybrid energy shifts which are quite similar in relative strength to our Monte Carlo results; this led Isgur and Paton to revise their adiabatic hybrid mass estimate upwards from 1.67 GeV to ~1.9 GeV [13]. The overall scale of adiabatic corrections quoted by Merlin and Paton [12] (see especially their Table 6) is about twice as large as we find numerically, but this may be due to their use of the large-N limit, whereas we have specialized to $N = 1$.

D. Physical hybrid masses

The flux tube results discussed in the previous section are not applicable to real hadrons because they do not include the color Coulomb interaction. Without the Coulomb interaction the flux tube at small R gives an SHO-like adiabatic potential [see $E_0(R)$ in Fig. 1], which leads to nearly equal S-P-D splittings in the spectrum of conventional $q\bar{q}$ mesons (as in Fig. 4). A realistic description of the S-P-D splittings requires the familiar "funnel-shaped" potential, in which linear confinement is augmented by a short ranged attraction.

In conventional potential models the Coulomb plus linear form

$$V_{q\bar{q}}(R) = -\frac{4}{3}\frac{\alpha_s}{R} + aR + V_0 \tag{42}$$

is most often used, with a string tension of $a \approx 0.9$–1.0 GeV/fm giving the best fit. Perturbative QCD predicts that the effective Coulomb interaction strength α_s should run with the scale of momentum of the scattered constituents, provided that we are well above any intrinsic mass scales. For resonance physics this requirement is obviously not satisfied, but there is nonetheless clear evidence for a rapid decrease of α_s with increasing quark mass; fits to spectroscopy typically require $\alpha_s \approx 0.6$–0.7 for $q = u, d, s$, $\alpha_s \approx 0.3$–0.4 for $q = c$, and $\alpha_s \approx 0.2$ for $q = b$.

For our realistic parameter set we assume constituent quark masses of $m_q = 0.33$, 0.55, and 1.5 GeV for $q = u(d)$, s, and c, and again set the string tension equal to $a = 1.0$ GeV/fm. In addition we include a color Coulomb and constant potential,

$$V_{q\bar{q}} = -\frac{4}{3}\frac{\alpha_s^{\rm ft}}{R} + V_0 , \tag{43}$$

in the flux tube quark Hamiltonian (2). The additive constant V_0 is found to be large and negative in potential models, and in the flux tube model is required in part to cancel the zero-point energies of the beads. The coefficient $-4/3$ multiplying α_s/r in the color Coulomb interaction merits additional comment. In constituent gluon models of hybrids the $q\bar{q}$ pair would be in a color octet, so the $-4/3$ would be replaced by $1/6$. In the flux tube model, in which gluonic excitations are presumed nonperturbative in α_s, it may be more realistic to use $-4/3$. This can be motivated by noting that at small R the lowest gluonic excitation is a color singlet $q\bar{q}$ pair (hence $-4/3$) plus a scalar glueball, rather than a $q\bar{q}$ color octet pair with a diverging $+1/6$ color Coulomb interaction [35].

The $\alpha_s^{\rm ft}$ in the $N = 1$ flux tube $V_{q\bar{q}}$ cannot be compared directly to the Coulomb plus linear α_s, because the fixed-N flux tube gives an SHO-like confining potential at short distances [see $E_0(R)$ in Fig. 1] in addition to the linear term which dominates at large R. Since $\alpha_s^{\rm ft}$ in the fixed-N flux tube model must cancel this additional contribution to produce a funnel-shaped potential comparable to the standard Coulomb plus linear form, it is larger than the potential model α_s.

We used multiplet-averaged E_S and E_P energies as input to fix $\alpha_s^{\rm ft}$ and V_0 in each flavor sector. The numbers used were $E_P - E_S = 0.62$ GeV for $q = u, d$ (from $I = 1$) and 0.45 GeV for c. The fitted values of $\alpha_s^{\rm ft}$ are 1.3 and 0.72 respectively, each determined to a few percent accuracy. The $E_P - E_S$ separation proved to be quite sensitive to the strength of the Coulomb potential. The constant V_0 was fixed separately for each flavor by using the spin-averaged masses $E_S^{(I=1)} = 0.63$ GeV and $E_S^{(c\bar{c})} = 3.07$ GeV as input. This required $V_0^{(I=1)} = -1.71$ GeV and $V_0^{(c\bar{c})} = -1.17$ GeV. Since these constant contributions cancel zero-point energies, they are not physically relevant. One might expect them to be roughly flavor independent, however, which can be achieved by increasing m_c to 1.8 GeV; the effect on the hybrid spectrum will be discussed subsequently. For $s\bar{s}$ we used the u, d parameters and simply increased the quark mass to $m_s = 0.55$ GeV.

The Monte Carlo technique was used to determine masses of $q\bar{q}$ and hybrid states up to $L = 3$. For $L > 0$ $q\bar{q}$ states we used

$$f^{(L,M)}(\theta,\phi) = P_L^M(\cos(\theta))\,\cos(M\phi) \tag{44}$$

in the guiding wave function (38) and the high statistics runs used $M = 0$. For the hybrids we again used the rigid-body angular wave function (41). Tests of node dependence were carried out by varying M. The simulations used the same statistics as the $\alpha_s = 0$ studies of the previous section, although we found that $\tau_1 = 5.0$ GeV^{-1} sufficed for convergence of level separations to within the statistical errors. These errors were typically about ± 5 MeV for quarkonium states and ± 10 MeV for hybrids. The guiding wave function parameters used in (34) were $\xi_{q\bar{q}} = 3/(2m_q\alpha_s^{\rm ft})$ (to give an accurate Coulomb wave function for S waves at short distance), and the flux tube length scale ξ was optimized numerically for each state. For all $q\bar{q}$ and $c\bar{c}$ states we found that $\xi = 1.5$ fm was nearly optimum. For $q\bar{q}$ hybrids we found $\xi = 1.8$ fm for $\Lambda = 1$ and 2.4 fm for $\Lambda = 2$. (Note that the higher flux tube excitation requires a larger length scale, as expected.) For $c\bar{c}$ hybrids we found slightly smaller flux tube length scales, $\xi = 1.6$ fm for $\Lambda = 1$ and 2.1 fm for $\Lambda = 2$. The quarkonium levels were again independent of M to within our statistical erors, but some bias was evident in the hybrids. This bias decreased with increasing m_q and m_b, as expected. The largest bias was found in the light ${}_1P$ hybrid, for which $E(M = 1) - E(M = 0) = 57(9)$ MeV, similar to our findings for $\alpha_s = 0$. This fell to 36(7) MeV for charmonium. The corresponding $E(M = 2) - E(M = 0)$ bias for ${}_1D$ was 24(13) MeV for $u\bar{u}$ and 18(9) MeV for $c\bar{c}$. Measurements with $\pm|M|$ appear to give equivalent results. For this work we average over measurements with all values of $|M| = 0$ to L; the discrepancies given above imply a systematic uncertainty of about ± 30 MeV for the u, d ${}_1P$ hybrid, ± 20 MeV for the ${}_1P$ $c\bar{c}$ hybrid, and rather less for the other states. This error could be reduced in future work through incorporation of improved nodal surfaces.

Our numerical results with the standard parameter set $(m_q, m_b, \alpha_s^{\rm ft}, a) = (0.33$ GeV, 0.2 GeV, 1.3, 1.0 GeV/fm) are shown in Fig. 5. The predicted D-wave $q\bar{q}$ mass of 1.66(1) GeV is quite reasonable, given the well-established D-wave candidates $\rho_3(1690)$, $\omega_3(1670)$, and $\pi_2(1670)$. The F-wave $q\bar{q}$ multiplet is predicted to lie at 2.03(2) GeV, in good agreement with the $a_4(2040)$, $a_3(2050)$, and $f_4(2050)$. The lightest hybrid multiplet, which has $\Lambda = 1$ and $L = 1$ (${}_\Lambda L = {}_1P$ in our notation), is at 1.90 GeV with these parameters. This is identical to the Isgur-Merlin-Paton prediction of 1.9 GeV

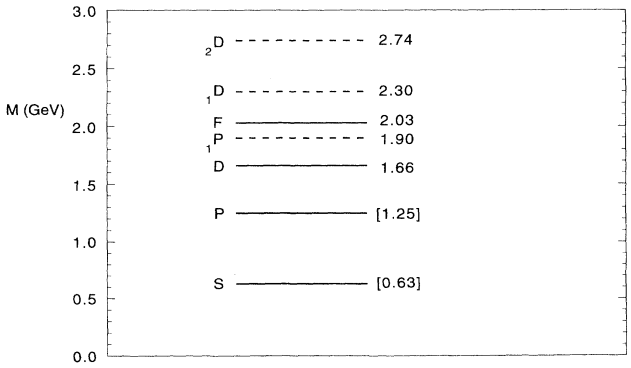

FIG. 5. The lightest $L = 0$–3 $q\bar{q}$ ($q = u, d$) and ${}_\Lambda L = {}_1P$, ${}_1D$, and ${}_2D$ hybrid masses from Monte Carlo data with physical parameters, $m_q = 0.33$ GeV, $m_b = 0.2$ GeV, $a = 1.0$ GeV/fm, $\alpha_s^{\rm ft} = 1.3$. Square brackets denote masses used as input.

[12,13]. Since we are using different versions of the flux tube model, this agreement is somewhat fortuitous, although we will show that our result is rather insensitive to parameter variations.

In view of the interest in the experimental hybrid candidate at 1775 MeV [4], which may have exotic $J^{PC} = 1^{-+}$ but 2^{-+} and 3^{++} are also possible, we also determined the mass of the radially excited $L = 2$ $q\bar{q}$ multiplet, which contains the first $I = 1$ 2^{-+} $q\bar{q}$ level expected above the $\pi_2(1670)$. (A 3^{++} $q\bar{q}$ state would require $L = 3$, and since this multiplet has well established members near 2.05 GeV we do not consider this a plausible $q\bar{q}$ assignment.) For the radial simulation we multiplied the $q\bar{q}$ guiding wave function $\psi_g^{(L)}$ in (38) by $|R - R_0|$, and varied the node radius R_0 until the energies determined by Monte Carlo simulations in the $R > R_0$ and $R < R_0$ regions were equal. This required $R_0 = 1.5$ fm and gave an energy of $E'_D \approx 2.3$ GeV, similar to potential model expectations [36] and far above the 1775 MeV state. This state is thus very unlikely to be a radially excited D-wave $q\bar{q}$.

We find that the first orbitally excited hybrid multiplet ($_1D$) is at 2.30 GeV, 400 MeV above the lightest ($_1P$) hybrids. The same numerical result was found earlier by Merlin [15] using the adiabatic approximation. This $_1D$ multiplet contains the J^{PC} states $(1,2,3)^{\pm\mp}$ and $2^{\pm\pm}$, which includes the exotics 1^{-+}, 2^{+-}, and 3^{-+}. This level is surprisingly high in mass, since a small orbital excitation gap has been anticipated for hybrids, due to the relatively flat hybrid adiabatic potential found by Perantonis and Michael [23] in heavy-quark lattice gauge theory. We shall see that the orbital excitation gap is somewhat smaller for $c\bar{c}$ hybrids in our model, so there is no serious inconsistency with HQLGT results. If the experimental hybrid candidates near 1.8 GeV [4] and 1.6–2.2 GeV [6] are confirmed, it may be useful to search for members of this $_1D$ hybrid multiplet near 2.2 GeV (about 0.4 GeV above $_1P$). A sequence of hybrids with higher orbital excitation is expected in the flux tube model, although these may be increasingly difficult to observe due to small matrix elements with light $q\bar{q}$ states.

We also determined the mass of the lightest $\Lambda = 2$ hybrid multiplet, $_2D$. These states are found to be quite high in mass, ≈ 2.75 GeV, so they should be irrelevant for light quark spectroscopy in the 2 GeV mass region. Merlin and Paton anticipate a lighter two-phonon hybrid multiplet, near 2.2 GeV in the adiabatic approximation. In their level the phonon angular momenta cancel ($\Lambda = 0$ "paraphononium"), whereas we have considered $\Lambda = 2$ "orthophononium." These $\Lambda = 0$ two-phonon states have conventional $q\bar{q}$ quantum numbers, which could complicate their identification.

The sensitivity of hybrid mass predictions to parameter variations is an important issue which has received little attention in previous flux tube studies. To investigate this we sequentially increased one parameter of the set $(m_q, m_b, \alpha_s^{\rm ft}, a)$ by 20%; recall that our standard parameter set (0.33 GeV, 0.2 GeV, 1.3, 1.0 GeV/fm) gave $(P, D, {}_1P, {}_1D)$ masses of ([1.25](input),1.66,1.90,2.30) GeV. [V_0 is always chosen to give $M_S = (3M_\rho + M_\pi)/4 = 0.63$ GeV.] The variations of these masses with parameters (with errors of typically ± 0.01 GeV) were

$$\Delta(M - M_S)(P, D, {}_1P, {}_1D)\ (\text{GeV}) = \begin{cases} (-0.01, -0.02, -0.01, -0.02) & (\Delta m_q/m_q = 0.2), \\ (-0.01, +0.01, -0.05, -0.03) & (\Delta m_b/m_b = 0.2), \\ (+0.07, +0.08, +0.06, +0.09) & (\Delta\alpha_s^{\rm ft}/\alpha_s^{\rm ft} = 0.2), \\ (+0.05, +0.11, +0.13, +0.16) & (\Delta a/a = 0.2). \end{cases} \tag{45}$$

This leads to several conclusions about the importance of parameter uncertainties in our flux tube spectrum. First, the level separations are evidently quite insensitive to variations in quark mass. Second, they are sensitive to changes in $\alpha_s^{\rm ft}$ and a, but the known P-S and D-S $q\bar{q}$ separations preclude any large changes in these parameters. In any case the hybrid and D-wave levels behave similarly under changes in $\alpha_s^{\rm ft}$ and a, so the predicted hybrid to D-wave separation is quite stable. It is the bead mass that leads to the largest uncertainty. The energies do not depend especially strongly on this parameter, but the hybrid and $q\bar{q}$ energy shifts have opposite signs. [This is more evident in (46) below.] Unfortunately the $q\bar{q}$ masses are quite insensitive to m_b, so ideally we would use a hybrid mass to determine m_b. To estimate the range of plausible hybrid masses as we vary m_b we consider the range $m_b = 0.2$–0.4 GeV; 0.2 GeV is our standard value and 0.4 GeV corresponds to a large flux tube length scale (see discussion in Sec. II B). Over this range of m_b we find the masses (with square brackets as input data)

$$(S, P, D, {}_1P, {}_1D)\ (\text{GeV}) = \begin{cases} ([0.63], [1.25], 1.66, 1.90, 2.30) & (m_b = 0.2\ \text{GeV}), \\ ([0.63], 1.27, 1.70, 1.78, 2.22) & (m_b = 0.4\ \text{GeV}). \end{cases} \tag{46}$$

With rounding to 0.1 GeV accuracy this leads to our final estimate of the lightest hybrid mass:

$$M({}_1P) = 1.8\text{–}1.9\ \text{GeV}\ . \tag{47}$$

The first orbitally-excited hybrid $_1D$ and the first $\Lambda = 2$ hybrid $_2D$ are expected at about 0.4 GeV and 0.8 GeV above the $_1P$ hybrid level respectively.

For $s\bar{s}$ quarkonia and hybrids we simply increased m_s to 0.55 GeV. The resulting level splittings were very similar to the results for u, d states. Using a P-wave $s\bar{s}$ mass of 1.50 GeV as input to fix V_0, our $s\bar{s}$ results are

$$(S, P, D, {}_1P, {}_1D)\ (\text{GeV}) = (0.87, [1.50], 1.88, 2.17, 2.54) \quad (m_b = 0.2\ \text{GeV}). \tag{48}$$

The only significant changes noted were a decrease in the D-wave level (relative to E_S) of $\Delta(E_D - E_S) = -0.02$ GeV and an increase in the ${}_1P$ level by 0.03 GeV. Thus we expect the first $s\bar{s}$ hybrid near $M_D(s\bar{s}) + 0.29$ GeV, about 50 MeV higher above the D-wave level than we found for the corresponding u, d states. The dependence on m_b was very similar to that found for u, d, so our final result for the first $s\bar{s}$ hybrid level ${}_1P$ was 2.1–2.2 GeV.

For charmonium and $c\bar{c}$ hybrids with our standard parameters $m_c = 1.5$ GeV, $m_b = 0.2$ GeV, $\alpha_s^{\text{ft}} = 0.72$, and $a = 1.0$ GeV/fm, we predict the following levels:

$$(S, P, D, {}_1P, {}_1D)\ (\text{GeV}) = ([3.07], [3.52], 3.77, 4.21, 4.48) \quad (m_b = 0.2\ \text{GeV}). \tag{49}$$

These are displayed in Fig. 6. Note that the predicted D-wave $c\bar{c}$ mass of 3.77 GeV is in good agreement with the experimental $\psi(3770)$. With these parameters we expect the lightest charmonium hybrid at 4.2 GeV. The first orbital excitation gap of $c\bar{c}$ hybrids in HQLGT was found to be 0.22 GeV by Perantonis and Michael [23] whereas we estimate 0.27 GeV; given the approximations this does not represent a serious discrepancy, although we shall see below that it is a rather stable prediction of this version of the flux tube model.

To test the sensitivity of these results to parameters we again increased each parameter in turn by +20%, which gives the mass shifts

$$\Delta(M - M_S)(P, D, {}_1P, {}_1D)\ (\text{GeV}) = \begin{cases} (+0.02, +0.03, +0.04, +0.04) & (\Delta m_c/m_c = 0.2), \\ (+0.01, +0.02, -0.05, -0.02) & (\Delta m_b/m_b = 0.2), \\ (+0.10, +0.13, +0.07, +0.11) & (\Delta\alpha_s^{\text{ft}}/\alpha_s^{\text{ft}} = 0.2), \\ (+0.04, +0.06, +0.14, +0.14) & (\Delta a/a = 0.2). \end{cases} \tag{50}$$

Thus for hybrid charmonium we reach similar conclusions regarding parameter uncertainties. The results are quite insensitive to m_c; increasing m_c from 1.5 GeV to 1.8 GeV only increases the first hybrid mass by 40 MeV. Since charm quark masses from 1.25 GeV (HQLGT [23]) to 1.77 GeV (flux tube [12–14]) have been used in the hybrid literature, it is reassuring to find that the lightest hybrid mass changes by only about 0.1 GeV over this wide range. As with light quarks we find that a and α_s^{ft} strongly affect the hybrid mass spectrum. These parameters, however, are tightly constrained by the known quarkonium spectrum. The largest uncertainty again comes from m_b, which is not very well determined by the $c\bar{c}$ spectrum nor by more general theoretical considerations. To test a wide range of possible values we again vary m_b over the range $m_b = 0.2$–0.4 GeV; with $m_b = 0.4$ GeV we find

$$(S, P, D, {}_1P, {}_1D)\ (\text{GeV}) = ([3.07], 3.54, 3.82, 4.08, 4.37) \quad (m_b = 0.4\ \text{GeV}). \tag{51}$$

Our final result for the lightest hybrid charmonium mass is thus

$$M({}_1P) = 4.1\text{–}4.2\ \text{GeV}\ , \tag{52}$$

and for charmonium we expect the orbital $({}_1D)$ and doubly excited $({}_2D)$ hybrids about 0.3 GeV and 0.7–0.8 GeV above the ${}_1P$ level, respectively.

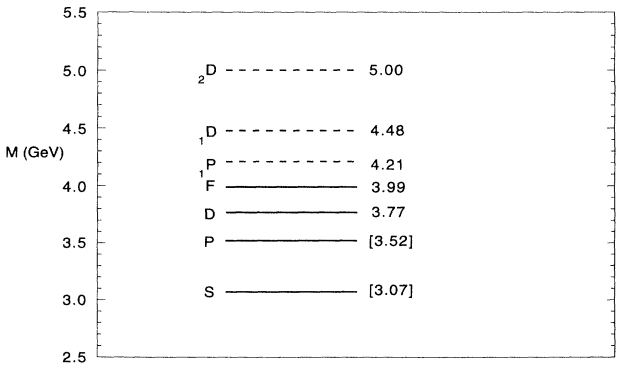

FIG. 6. Charmonium $c\bar{c}$ and hybrid masses, legend as in Fig. 5. Parameters modified for charmonium are $m_c = 1.5$ GeV and $\alpha_s^{\text{ft}} = 0.72$.

V. PHENOMENOLOGICAL IMPLICATIONS

We have studied the fixed-N version of the flux tube model, principally the $N = 1$ case, as a numerically tractable version of this type of hadron model.

The ability to reproduce the spectrum of conventional quarkonia with $N = 1$ is of interest in its own right. It suggests that we have a unified picture of both quark and flux tube excitation spectra, thereby generating some confidence in the predicted hybrid masses. In this final section we summarize implications of these results. Of course the predictions of the model for $N > 1$ remain interesting, especially for the relatively large light hadrons, because the characteristic transverse size of the flux tube and hence the most realistic N are not well determined. We discuss some preliminary Monte Carlo results for the cases $N = 2$ and $N = 3$ in a footnote [37].

Our studies suggest that the adiabatic approximation, used in previous analyses of hybrid meson masses in the flux tube model, underestimates the hybrid mass scale. Our conclusions substantiate previous analytical estimates of corrections to the adiabatic approximation [12,14], and lead to hybrid masses that are ≈ 0.1 GeV above the predictions of quenched heavy-quark lattice QCD, but are consistent with these lattice results given

their estimated corrections to the quenched approximation.

In contrast to the light quark sector, in which flavor mixing in nonexotics may be important and the $q\bar{q}$ spectrum itself is rather controversial, in heavy-quark systems the $Q\bar{Q}$ spectroscopy is relatively straightforward and special opportunities ensue for the detection of hybrids. Our results support the expectation that heavy hybrids H_Q appear at masses of

$$M(H_Q) \approx M_0(Q\bar{Q}) + 1 \text{ GeV} . \quad (53)$$

An important feature in heavy $Q\bar{Q}$ spectroscopy is the existence of narrow states spanning a mass range from $\approx M_0(Q\bar{Q})$ through ≈ 1 GeV up to the two-body open-flavor threshold (i.e., ψ to $D\bar{D}$ or Υ to $B\bar{B}$). So for charmonium hybrids, for example, one anticipates H_c states in the resonance region not far above the open charm threshold of 3.73 GeV. In our simulations we actually find the first charmonium hybrids at $M(H_c) = 4.1$–4.2 GeV.

Such a prediction is particularly exciting. Charmonium spectroscopy is rather well understood up to about 3.8 GeV, so searches for unusual states should be straightforward near this mass. Since only a few open charm channels occur below 4.3 GeV, for a considerable range of hybrid masses one might anticipate rather narrow hybrid resonances. This possibility receives additional support from the flux tube model [16,17], which predicts that the dominant two body decay modes of the lowest lying hybrids are an $L = 0$ and $L = 1$ $q\bar{q}$ meson pair. These $S + P$ thresholds are rather high in mass, about 4.3 GeV for $c\bar{c}$ hybrids and 11.0 GeV for $b\bar{b}$ hybrids. The possibility that relatively narrow hybrid charmonium states may exist within this 3.8–4.3 GeV window provides an exciting opportunity for e^+e^- facilities such as BEPC, KEK, and a Tau-Charm Factory. If there are indeed hybrids at these masses, one expects that they should be produced copiously by gluon fragmentation at large momentum transfers, for example at the Tevatron. Detection of the ψ or $\psi(3685)$ as a signature of hadronic cascade decays of metastable hybrid charmonia has been discussed in Ref. [10]. (A double cascade from the $c\bar{c}$ continuum to a hybrid and thence to $c\bar{c}$ was proposed for a Tau-Charm Factory by Bugg; see Ref. [38].) In practice the usefulness of cascade decays in hybrid searches will depend on their branching fractions to conventional quarkonia.

Determination of the production and decay characteristics of hybrid states is beyond the scope of this study, but we note in passing that progress in this area has been made recently by analytical modelling of flux tube excitations [17,18]. In these references the decay amplitudes of some recently discovered 1^{-+}, 0^{-+}, 1^{--}, and 2^{-+} u,d-flavored mesons were found to be in good agreement with the predicted properties of hybrid mesons, so the flux tube model may be a useful guide to strong decay modes as well as masses. Widths of the hybrid charmonia calculated in this model support the suggestion that some of these $c\bar{c}$ hybrids are likely to be narrow.

The production of 1^{--} charmonium vector hybrids seems especially promising. As the flux tube has an orbital excitation about the $q\bar{q}$ axis, and the $q\bar{q}$ themselves have an effective centrifugal barrier due to the flux tube angular momentum, which suppresses the radial $q\bar{q}$ wave function at small r, we anticipate that the e^+e^- widths $\Gamma_{ee}(V_c)$ should be significantly smaller than those of the conventional $c\bar{c}$ states ψ and $\psi(3686)$.

In light quark systems this wave function suppression is not dramatic (see for example the Particle Data Group summary of $V \to e^+e^-$ [39] for $L = 0$ and $L = 2$ $q\bar{q}$ states following the analyses of Ref. [40]), and so we anticipate a significant light hybrid leptonic width $\Gamma_{ee}(\rho_g)$. The principal difficulty here may lie in distinguishing between light conventional and hybrid vector states unambiguously. The recent analyses of the light vector sector by Donnachie and Kalashnikova [41] actually do support the presence of additional vector states, some of which they suggest may be hybrids.

The recent studies of hybrid decays in the flux tube model [17,18] may allow tests of these possible light vector hybrids. Since the $q\bar{q}$ pair in V_g has $S_{q\bar{q}} = 0$, whereas conventional $q\bar{q}$ vector states (either $^3S_1$ or $^3D_1$) have $S_{q\bar{q}} = 1$, there are characteristic selection rules for decays that discriminate between these spin-singlet and -triplet states. In particular, if the $q\bar{q}$ are in a spin singlet (as in the V_g vector hybrid case) the flux tube decay model forbids decays into final states of two spin-singlet mesons.

For $J^{PC} = 1^{--}$ states this selection rule distinguishes rather clearly between conventional and hybrid vector mesons. It implies that in the decays of a light ρ_g hybrid $\rho_g \not\to h_1\pi$, although $\rho_g \to a_1\pi$ is allowed. Analogously, $\omega_g \not\to b_1\pi$ for hybrid 1^{--} ω_g decays; this is opposite to the case of conventional $^3L_1$ $q\bar{q}$ mesons, for which the $a_1\pi$ channel is suppressed relative to $h_1\pi$ or $b_1\pi$ [42,43]. The extensive analysis of data in Ref. [40] revealed the clear presence of a $\rho(1450)$ [39] with a strong $a_1\pi$ mode but no evidence for $h_1\pi$, in accord with expectations for a hybrid. Furthermore, Ref. [40] finds an $\omega(1440)$ with no evidence for decays into $b_1\pi$, again in conflict with expectations for conventional $q\bar{q}$ ($^3S_1$ or $^3D_1$) states but in accord with predictions for hybrid decays.

The branching fractions reported for the $\rho(1450)$ [40] (see also [18]) suggest that there may be mixing between ρ_g and radial ρ basis states in this region. If these hybrid states near 1.5 GeV are confirmed, this mixing may explain the low mass relative to the 1.8–2.0 GeV typical of other hybrid candidates. There may also be significant spin-dependent mass shifts in hybrids that were not incorporated in the present study, which reduce spin-singlet masses (such as V_g) relative to the spin-triplet states ($0^{-+/-+}, 1^{-+/+-}, 2^{-+/+-}$). To test this possibility, analogous experimental investigations of 1^{--} hybrid charmonia in e^+e^- would be very useful. In contrast, in $b\bar{b}$ systems the suppressed wave function at contact is expected to make H_b hybrids essentially absent in e^+e^- annihilation. For this reason the charmonium system may be optimal for hybrid searches; conventional $c\bar{c}$ spectroscopy is reasonably well established, and since the D-wave coupling $\Gamma_{ee}(\psi(3770))$ is not negligible, it may be

possible to observe a moderately suppressed V_c vector hybrid signal in e^+e^- annihilation at a Tau Charm Factory [38]. Diffractive photoproduction of charmonium hybrids, $\gamma^* P \to XP$, may also be possible, for example, at HERA.

If the mass of the V_c is indeed below or near 4.3 GeV ($D^{**}\bar{D}$ threshold), then hadronic cascades to conventional charmonium states, in particular the $\psi(3097)$ and $\psi(3685)$, may be important and could provide a good tag [10]. The E835 experiment at Fermilab may be able to observe production of hybrid charmonium through hadronic cascade decays to $\psi\pi\pi$ and $\psi\eta$.

For hybrids which lie above $D^{**}\bar{D}$ threshold, heavy-quark symmetry or detailed decay models may be used to distinguish the spin-singlet H_c from the spin-triplet ψ states through their decay systematics. More detailed theoretical study of this and related questions is now warranted.

To summarize, we find that heavy-quark hybrids in the flux tube model lie below $S+P$ thresholds, and for hybrid charmonium this implies that the lightest states should have rather narrow widths. We anticipate that production by gluon jets may be particularly promising and for this case some quantitative estimates already exist [10] based on the masses found here.

In conclusion, we find that the lightest hybrid masses in the flux tube model are $M(H_{u,d}) = 1.8$–1.9 GeV and $M(H_c) = 4.1$–4.2 GeV. These results, combined with recent detailed studies of hybrid decay modes [17,18], provide a clear set of theoretical predictions for hybrids for comparison with experiment.

ACKNOWLEDGMENTS

We would like to acknowledge useful discussions or communications with E.S. Ackleh, G. Condo, J. Govaerts, N. Isgur, S. Narison, P.R. Page, and J. Paton. This research was sponsored in part by the European Community Human Mobility program EURODAFNE, Contract No. CHRX-CT92-0026, and the United States Department of Energy under Contract No. DE-AC05-840R21400 managed by Martin Marietta Energy Systems Inc. at Oak Ridge National Laboratory.

[1] For recent reviews of spectroscopy from lattice gauge theory see S.R. Sharpe, in *CP Violation and the Limits of the Standard Model*, Proceedings of the Theoretical Advanced Study Institute, Boulder, Colorado, 1994 (World Scientific, Singapore, 1995); D. Weingarten, in *Lattice '93*, Proceedings of the International Symposium, Dallas, Texas, edited by T. Draper *et al.* [Nucl. Phys. B (Proc. Suppl.) **34**, 29 (1994)]. Recent high-statistics lattice glueball results include G. Bali *et al.*, Phys. Lett. B **309**, 378 (1993), $M(0^{++}) = 1.55(5)$ GeV; H. Chen *et al.*, in *Lattice '93*, this reference, $M(0^{++}) = 1.740(71)$ GeV and $M(2^{++}) = 2.359(128)$ GeV. Two-pseudoscalar decay widths are discussed by J. Sexton *et al.*, in *Lattice '94*, Proceedings of the International Symposium, Bielefeld, Germany, edited by F. Karsch *et al.* [Nucl. Phys. B (Proc. Suppl.) **42** (1995)].

[2] V.V. Anisovich *et al.*, Phys. Lett. B **323**, 233 (1994); C. Amsler, in *Proceedings of the XXVII International Conference on High Energy Physics*, Glasgow, Scotland, 1994, edited by P.J. Bussey and I.G. Knowles (IOP, London, 1995); see also C. Amsler and F.E. Close, "Evidence for Glueballs," Rutherford Laboratory and CERN Report No. CCL-TR-95-003, 1995 (unpublished).

[3] J.P. Peigneux *et al.*, CERN Report No. CERN-SPSLC 94-22, CERN-P281, 1994 (unpublished).

[4] G. Condo *et al.*, Phys. Rev. D **43**, 2787 (1991); the same state may have been seen earlier by D. Aston *et al.*, Nucl. Phys. **B189**, 15 (1981).

[5] G.M. Beladidze *et al.*, Phys. Lett. B **313**, 276 (1993).

[6] J.H. Lee *et al.*, Phys. Lett. B **323**, 227 (1994).

[7] D. Alde *et al.*, Phys. Lett. B **205**, 397 (1988).

[8] H. Aoyagi *et al.*, Phys. Lett. B **314**, 246 (1993).

[9] CDF Collaboration, M. Mangano, in Proceedings of the XXIX Rencontres de Moriond, Méribel (unpublished); in *Proceedings of the 27th International Conference on High Energy Physics* [2].

[10] F.E. Close, Phys. Lett. B **342**, 369 (1995).

[11] N. Isgur and J. Paton, Phys. Lett. **124B**, 247 (1983).

[12] J. Merlin and J. Paton, J. Phys. G **11**, 439 (1985).

[13] N. Isgur and J. Paton, Phys. Rev. D **31**, 2910 (1985).

[14] J. Merlin and J. Paton, Phys. Rev. D **35**, 1668 (1987).

[15] J. Merlin, Ph.D. thesis, Oxford University; J. Paton (personal communication).

[16] N. Isgur, R. Kokoski, and J. Paton, Phys. Rev. Lett. **54**, 869 (1985).

[17] F.E. Close and P.R. Page, Nucl. Phys. **B443**, 233 (1995).

[18] F.E. Close and P.R. Page, Phys. Rev. D **52**, 1706 (1995).

[19] T. Barnes, Ph.D. thesis, Caltech, 1977; Nucl. Phys. **B158**, 171 (1979); T. Barnes and F.E. Close, Phys. Lett. **116B**, 365 (1982); M. Chanowitz and S.R. Sharpe, Nucl. Phys. **B222**, 211 (1983); T. Barnes, F.E. Close and F. deViron, *ibid.* **B224**, 241 (1983); M. Flensburg, C. Peterson, and L. Sköld, Z. Phys. C **22**, 293 (1984).

[20] P. Hasenfratz, R.R. Horgan, J. Kuti, and J.-M. Richard, Phys. Lett. **95B**, 299 (1980).

[21] D. Horn and J. Mandula, Phys. Rev. D **17**, 898 (1978).

[22] M. Tanimoto, Phys. Lett. **116B**, 198 (1982); Phys. Rev. D **27**, 2648 (1983); A. LeYaouanc, L. Oliver, O. Pène, J.-C. Raynal, and S. Ono, Z. Phys. C **28**, 309 (1985); F. Iddir, A. LeYaouanc, L. Oliver, O. Pène, J.-C. Raynal, and S. Ono, Phys. Lett. B **205**, 564 (1988); S. Ishida, H. Sawazaki, M. Oda, and K. Yamada, Phys. Rev. D **47**, 179 (1992); Prog. Theor. Phys. **82**, 119 (1989).

[23] S. Perantonis and C. Michael, Nucl. Phys. **B347**, 854 (1990), and references cited therein.

[24] See, for example, T. Barnes, in *Proceedings of the Third Workshop on the Tau-Charm Factory,* Marbella, Spain, 1993, edited by J. Kirkby and R. Kirkby (Editions Fron-

tieres, Gif-sur-Yvette, France, 1994); F.E. Close, *ibid.*; T. Barnes, in Proceedings of the Conference on Exclusive Reactions at High Momentum Transfers, Marciana Marina, Elba, Italy, 1993 (unpublished); F.E. Close, Rep. Prog. Phys. **51**, 833 (1988); C. Dover, in Proceedings of the Second Biennial Conference on Low Energy Antiproton Physics, Courmayeur, 1992 (unpublished); A. Dzierba, in *Future Directions in Particle and Nuclear Physics at Multi-GeV Hadron Beam Facilities*, Proceedings of the Workshop, Upton, New York, 1993, edited by D. Geesaman (BNL Report No. 52389, Upton, 1993); S. Godfrey, in *Glueballs, Hybrids, and Exotic Hadrons,* edited by S.-U. Chung, AIP Conf. Proc. No. 185 (AIP, New York, 1989); D. Hertzog, Nucl. Phys. **A558**, 499c (1993); N. Isgur, in *Proceedings of the XXVI International Conference on High Energy Physics*, Dallas, Texas, 1992, edited by J. Sanford, AIP Conf. Proc. No. 272 (AIP, New York, 1993); G. Karl, Nucl. Phys. **A558**, 113c (1993).

[25] I.I. Balitsky, D.I. Dyakanov, and A.V. Yung, Phys. Lett. **112B**, 71 (1982); Sov. J. Nucl. Phys. **35**, 761 (1982); Z. Phys. C **33**, 265 (1986).

[26] J.I. Latorre, S. Narison, P. Pascual, and R. Tarrach, Phys. Lett. **147B**, 169 (1984); J.I. Latorre, P. Pascual, and S. Narison, Z. Phys. C **34**, 347 (1987); S. Narison, *QCD Spectral Sum Rules*, Lecture Notes in Physics Vol. 26 (World Scientific, Singapore, 1989), p. 375.

[27] J. Govaerts, F. deViron, D. Gusbin, and J. Weyers, Phys. Lett. **128B**, 262 (1983); **136B**, 445(E) (1983); J. Govaerts, L.J. Reinders, H.R. Rubinstein, and J. Weyers, Nucl. Phys. **B258**, 215 (1985); J. Govaerts, L.J. Reinders, and J. Weyers, *ibid.* **B262**, 575 (1985); J. Govaerts, L.J. Reinders, P. Francken, X. Gonze, and J. Weyers, *ibid.* **B284**, 674 (1987).

[28] J. Govaerts, F. deViron, D. Gusbin, and J. Weyers, Nucl. Phys. **B248**, 1 (1984).

[29] F. deViron and J. Govaerts, Phys. Rev. Lett. **53**, 2207 (1984).

[30] J.H. Merlin and J. Paton, Phys. Rev. D **36**, 902 (1987).

[31] See, for example, J. Wosiek and R.W. Haymaker, Phys. Rev. D **36**, 3297 (1987); A. DiGiacomo, M. Maggiore, and S. Olejnik, Phys. Lett. B **236**, 199 (1990); H.D. Trottier and R.M. Woloshyn, Phys. Rev. D **48**, 2290 (1993).

[32] P. Gnädig, P. Hasenfratz, J. Kuti, and A.S. Szalay, Phys. Lett. **64B**, 62 (1976).

[33] T. Barnes, G.J. Daniell, and D. Storey, Nucl. Phys. **B265** [FS15], 253 (1986). Since we calculate only energies in this flux tube simulation, we can reduce statistical errors by using only the "diagonal weight," as discussed in [34].

[34] T. Barnes and D. Kotchan, Phys. Rev. D **35**, 1947 (1987).

[35] N. Isgur (personal communication). We have also carried out Monte Carlo simulations of the case $+\alpha_s^{\rm ft}/6r$ to test the sensitivity of our results for the hybrid masses to the Coulomb potential assumed. We find that, despite the centrifugal barrier, the hybrid masses are rather sensitive to the Coulomb term, and the first two ($_1P$ and $_1D$) hybrid levels increase from (1.90 GeV, 2.30 GeV) to (2.26 GeV, 2.60 GeV) for light quarks and from (4.21 GeV, 4.48 GeV) to (4.60 GeV, 4.71 GeV) for $c\bar{c}$. Since we believe that the large values of $\alpha_s^{\rm ft}$ required in the model to fit quarkonium spectroscopy are actually compensating for the slow onset of linear confinement in the $N = 1$ potential evident in $E_0(R)$ in Fig. 1, these increases are presumably overestimates by about a factor of $\alpha_s^{\rm ft}/\alpha_s \approx 2$; so our best estimates of the $_1P$ hybrid masses with $+\alpha_s/6r$ are $\approx$ 2.1 GeV and $\approx$ 4.4 GeV for $q\bar{q}$ and $c\bar{c}$ hybrids, respectively. If the hybrids are found at these higher masses, the possibility of a repulsive Coulomb interaction should be investigated in more detail.

[36] In a nonrelativistic Coulomb plus linear potential model with $\alpha_s = 0.6$, $a = 0.9$ GeV/fm, $m_q = 0.33$ GeV, and again using the spin-averaged $M(\rho,\pi) = 0.63$ GeV to fix $V_0 = -0.82$ GeV, we find $M(D) = 1.66$ GeV and $M(D') = 2.31$ GeV, and a node in the D' wave function at $R_0 = 1.47$ fm. S. Godfrey and N. Isgur, Phys. Rev. D **32**, 189 (1985), quote a much lower $^1D_2'$ mass of 2.13 GeV. The string tension of $a = 1.0$ GeV/fm we used as our standard value in the flux tube model may be too large (0.9 GeV/fm is more conventional), and the radial excitations are more sensitive to this difference than the other $q\bar{q}$ states, which we found to be in good agreement with experiment given 1.0 GeV/fm. If we reduce the string tension in the $N = 1$ flux tube model to the rather low value of 0.8 GeV/fm, we find a mass of $M(D') = 2.1$ GeV, similar to Godfrey and Isgur. However the D-wave mass is then unacceptably low, $M(D) = 1.54$ GeV. The actual D' 2^{-+} $q\bar{q}$ state is presumably near 2.2 GeV, with an uncertainty of at most about 0.1 GeV.

[37] In a fixed-N flux tube model with a conventional string tension of $a \approx 1$ GeV/fm, and with bead masses comparable to light constituent quark masses, one must keep N relatively small; otherwise the large-amplitude configurations of the flux tube in its ground state are complicated proteinlike jumbles rather than a linear string, and this jumbled flux tube has a small excitation energy. To test the sensitivity of our results to moderate increases in N we carried out Monte Carlo simulations of light quark systems with $N = 2$ and $N = 3$, and found that the energies are actually rather similar to $N = 1$. We again used spin-averaged values of $M(P) = 1.25$ GeV and $M(S) = 0.63$ GeV as input to determine α_s and V_0. (As before we used $a = 1.0$ GeV/fm and $m_b = 0.2$ GeV, and these simulations used magnetic quantum number $M = 0$.) Both $N = 2$ and $N = 3$ required a very large $\alpha_s^{\rm ft} \approx 1.7$ to compensate for the shallow small-r confining potential. The predictions for the $D(q\bar{q})$, $_1P$(hybrid), and $F(q\bar{q})$ masses were 1.65, 1.70, and 1.99 GeV for $N = 2$ and 1.60, 1.65, and 1.91 GeV for $N = 3$, with statistical errors of about ± 0.02 GeV. A deterioration in the $q\bar{q}$ spectrum due to the slower onset of linear confinement in the larger-N string is clearly evident by $N = 3$, which underestimates the $L = 3$ mass by $\approx$ 130 MeV. There is a decrease in the first hybrid mass in both the $N = 2$ and $N = 3$ models relative to $N = 1$; it is predicted to be about 50 MeV above the $q\bar{q}$ D-wave states.

[38] F.E. Close, in *Proceedings of the Third Workshop on the Tau-Charm Factory* [24], p. 73; T. Barnes, *ibid.*, p. 41.

[39] Particle Data Group, L. Montanet *et al.*, Phys. Rev. D **50**, 1173 (1994).

[40] A.B. Clegg and A. Donnachie, Z. Phys. C **42**, 455 (1994).

[41] A. Donnachie and Yu. Kalashnikova, Z. Phys C **59**, 621 (1993); A. Donnachie, Yu. Kalashnikova, and A. Clegg, *ibid.* **60**, 187 (1993).

[42] G. Busetto and L. Oliver, Z. Phys. C **20**, 247 (1983).

[43] R. Kokoski and N. Isgur, Phys. Rev. D **35**, 907 (1987).